Labile iron pool dynamics do not drive ferroptosis potentiation in colorectal cancer cells

Varun Ponnusamy[1], Deahzana R. Randall[1], Zheng Hong Lee[2], Nupur K. Das[1], Liang Zhao[1], Kathryn Buscher[1], Sumeet Solanki[1], Adam R. Renslo[3], Peggy P. Hsu[4,5]*, Yatrik M. Shah[1,4,6]*
[1] Department of Molecular and Integrative Physiology, University of Michigan, Ann Arbor, MI, USA.
[2] Graduate Program of Immunology, University of Michigan, Ann Arbor, MI, USA
[3] Department of Pharmaceutical Chemistry, University of California, San Francisco, San Francisco, California, USA.
[4] Rogel Cancer Center, University of Michigan Medical School, Ann Arbor, MI, USA
[5] Department of Internal Medicine, Division of Hematology and Oncology, University of Michigan Medical School, Ann Arbor, MI, USA
[6] Department of Internal Medicine, Division of Gastroenterology, University of Michigan Medical School, Ann Arbor, MI, USA
* Correspondence: shahy@umich.edu and hsupe@med.umich.edu

Abstract

Colorectal cancer (CRC) is the second leading cause of cancer-related mortality in the United States. CRC tumors exhibit aberrant iron accumulation, which supports tumor cell proliferation through multiple metabolic pathways. However, the oncogenic benefits of elevated iron must be counterbalanced by its potential to catalyze oxidative damage via reactive oxygen species generated from labile, redox-active iron. Ferroptosis is a regulated, non-apoptotic form of cell death characterized by iron-dependent lipid peroxidation. This process is tightly controlled by the selenoenzyme glutathione peroxidase 4 (GPX4), which reduces lipid peroxides and can be pharmacologically inhibited by agents such as RSL3 and JKE1674. A key source of redox-active iron is the labile iron pool (LIP), yet its role in regulating ferroptosis remains incompletely defined. To examine this, we supplemented CRC cells with exogenous iron following pharmacologic induction of ferroptosis. Iron supplementation significantly reduced cell viability, suggesting that expansion of the LIP potentiates ferroptotic cell death. However, whether ferroptosis is accompanied by dynamic changes in the LIP, and if such changes are mechanistically required for its potentiation, was unknown. To further characterize this response, we profiled the expression of iron regulatory genes under ferroptotic conditions and observed no change in transcriptional response in iron homeostasis genes. When using a fluorescent probe for labile iron, we found that the LIP did not measurably increase during ferroptosis induction. These findings suggest that the LIP itself does not expand after the initiation of ferroptosis to become the primary driver of ferroptotic potentiation.

Introduction

Iron is an essential micronutrient that supports a wide range of cellular processes[1]. Given that both iron deficiency and overload can be harmful, iron levels are tightly regulated. The intestine plays a central role in this regulation, as it is the sole site of dietary iron absorption and the gateway for systemic iron distribution to peripheral tissues. Intestinal epithelial cells are exposed to two principal sources of iron: luminal dietary iron and iron derived from the systemic circulation. In the intestine, iron enters epithelial cells in its ferric (Fe^{3+}) form either apically via divalent metal transporter 1 (DMT1; Slc11a2) following reduction to the ferrous (Fe^{2+}) state, or basolaterally via transferrin-bound iron through the transferrin receptor (TFRC)[2,3]. Once inside the cell, iron is reduced to its ferrous form and is either incorporated into iron-dependent enzymes and cofactors or trafficked to the mitochondria for utilization[4]. Due to its redox

reactivity and potential to generate reactive oxygen species (ROS), intracellular iron is tightly controlled. Excess iron is either exported by the basolateral iron transporter ferroportin (FPN)[5] or stored within the protein complex ferritin (FTN)[6]. Under conditions of increased demand, stored iron can be mobilized through ferritinophagy, a selective autophagic process mediated by the cargo receptor nuclear receptor coactivator 4 (NCOA4)[7,8]. A central component of cellular iron regulation is the labile iron pool (LIP). The LIP is a cytosolic, redox-active, and readily chelatable pool of ferrous iron that serves as the key bioavailable iron reservoir.

A form of regulated, non-apoptotic cell death, known as ferroptosis, is characterized by its dependence on iron and its initiation through the accumulation of lipid peroxides[9,10]. The LIP plays a central role in ferroptosis by catalyzing the decomposition of hydrogen peroxide and oxygen via the Fenton reaction[11], generating highly reactive hydroxyl and hydroperoxyl radicals. These reactive oxygen species (ROS) cause oxidative damage to cellular membranes, particularly through the peroxidation of polyunsaturated fatty acids in membrane phospholipids, ultimately compromising membrane integrity and triggering ferroptotic cell death[12].

Ferroptosis research thus far has relied on synthetic small molecules known to induce ferroptotic cell death. Only recently have endogenous regulators of ferroptosis begun to be identified[13]. There remains a need to better understand endogenous mechanisms that mediate ferroptosis, including the role of iron itself, an underexplored but potentially critical regulator. Notably, certain cancers, such as colorectal cancer (CRC), exhibit a strong dependence on iron for growth, and are potentially susceptible to ferroptosis-based therapies[14–17]. Previous studies have shown that LIP is increased during ferroptosis; however, these findings primarily rely on iron-chelating methods to quantify the LIP, techniques that may inadvertently affect measurements and confound interpretation[18,19]. Gaining deeper insight into ferroptosis and the role of iron in its regulation may offer novel therapeutic strategies for CRC and other iron-dependent cancers.

In this study, we demonstrate that supplementation with exogenous free iron significantly enhances ferroptosis when combined with established ferroptotic inducers in multiple human CRC cell lines. To determine whether the LIP increases to potentiate ferroptosis via endogenous mechanisms, we investigated whether the LIP is naturally altered during ferroptosis. This was accomplished by profiling the expression of key iron homeostasis genes and using a reactivity-based probe to detect subtle changes in the LIP. Surprisingly, our analysis revealed no significant endogenous increase in the LIP during ferroptosis. These findings suggest that, contrary to expectations, the LIP remains relatively stable in the absence of exogenous iron manipulation and that additional regulatory mechanisms beyond iron availability may be required to effectively drive ferroptotic cell death.

Results

Exogenous iron sensitizes CRC cells to JKE-induced ferroptosis

The selenoprotein glutathione peroxidase 4 (GPX4) is a central regulator of ferroptosis[20]. Although inhibition of GPX4 is widely accepted as a mechanism to induce ferroptosis, we have previously shown that the commonly used GPX4 inhibitor RSL3 exhibits off-target effects and non-specific inhibition across the selenoproteome, including thioredoxin peroxidases[21]. We therefore utilized a more specific, next-generation GPX4 inhibitor, JKE1674 for our experiments.

Among the CRC cell lines, HCT116 and SW480 have been reported to be relatively resistant to ferroptosis inducers, whereas RKO is highly sensitive[17,21]. We found that JKE1674-mediated GPX4 inhibition was less potent in HCT116, SW480, and RKO compared to other ferroptosis

inducers[21] (Figure 1A, S1A). To determine whether manipulating the labile iron pool could sensitize cells to JKE1674 (0.625, 1.25, 2.5 μM), we co-treated cells with ferric ammonium citrate (FAC) at increasing concentrations (250, 500, and 1000 μM). The fibrosarcoma cell line HT1080, a well-established ferroptosis sensitive cell line[13], was included as a positive control. Exogenous iron significantly reduced cell viability in the ferroptosis-resistant CRC lines HCT116 and SW480, particularly at the highest FAC concentration (Figure 1B).

To quantify the interaction between FAC and JKE1674, we performed synergy analysis using the Bliss independence dose-response surface model[22]. This model assumes that two agents with independent mechanisms act additively unless synergy or antagonism is present. A synergy score above 10 indicates synergy, between -10 and 10 suggests additivity, and below -10 indicates antagonism. Our growth assays demonstrated synergistic interactions between FAC and JKE1674 across various concentrations in all four cell lines examined (Figure 1C).

Exogenous iron potentiates RSL3 and IKE-induced ferroptosis in CRC cells

Next, we tested whether FAC could potentiate two other ferroptotic inducers, RSL3 and the SLC7A11 inhibitor, imadazole ketone erastin (IKE) (Figure 2A, 2B). Co-treatment of HCT116 and RKO cells with RSL3 (1, 0.5, 0.25 μM) and FAC resulted in a dose-dependent decrease in cell viability. In contrast, SW480 cells, which are highly resistant to ferroptosis, did not exhibit enhanced sensitivity to either RSL3 or IKE upon FAC addition.

Ferroptosis can also be triggered by inhibition of the cystine/glutamate antiporter SLC7A11, which increases lipid peroxidation[9,23]. Notably, FAC potentiated IKE-induced cell death in the SW480 cell line. HCT116 cells showed a trend toward decreased viability at lower IKE concentrations, similar to effects seen in RKO and HT1080 cells (Figure 2B, S2B).

To quantify these interactions, we again applied the Bliss independence dose-response surface model. Co-treatment with RSL3 and FAC demonstrated strong synergy in HCT116 cells and additive effects in the remaining lines (Figure 2C). For IKE, synergistic effects were observed in SW480 and RKO, with additive responses in HCT116 and HT1080 (Figure 2D). Together, these results show that increasing the labile iron pool through exogenous iron supplementation can potentiate ferroptosis both through GPX4-dependent and GPX4-independent mechanisms.

Iron homeostatic genes are not altered following RSL3, JKE, and IKE-induced ferroptosis

In the intestine, iron is imported and exported through several key transporters DMT1, TFRC, and FPN (the only known mammalian iron exporter). FTN serves as the primary intracellular iron storage protein, sequestering excess iron from the LIP[1,24]. The expression of these iron homeostasis genes is regulated by iron regulatory proteins (IRPs), a class of RNA-binding proteins that control translation by binding to iron-responsive elements (IREs) within the untranslated regions (UTRs) of target mRNAs[25,26]. Depending on the location of IREs in the 3′ or 5′ UTR, IRP binding can upregulate or downregulate the expression of DMT1, TFRC, FPN, and ferritin heavy chain (FTH1) during systemic iron deficiency or overload[27,28].

In addition to IRPs, iron homeostasis genes are transcriptionally regulated by transcription factors. Hypoxia-inducible factor (HIF)-2α and nuclear factor erythroid 2–related factor (NRF)-2 bind to hypoxia response elements and antioxidant response elements, respectively, particularly under conditions of hypoxia or oxidative stress[14,29–32]. While these regulatory systems maintain iron balance under physiological conditions, it is unclear whether they become dysregulated and contribute to ferroptosis pathogenesis.

It is widely assumed, but not rigorously tested, that ferroptosis is accompanied by an endogenous increase in the LIP, which would sensitize cells to iron-dependent lipid peroxidation [18,19]. To investigate this, we examined the expression of iron homeostasis genes (DMT1, TFRC, FTH1, and FPN) following induction of ferroptosis. Quantitative RT-PCR was performed 16 hours after treatment with three distinct ferroptosis inducers (Figure 3). Surprisingly, ferroptosis induction did not result in significant transcriptional changes in iron homeostasis genes, except in SW480 cells treated with RSL3 (Figure 3A) and in HT1080 cells treated with IKE (Figure 3B). These findings suggest that, despite the central role of iron in ferroptosis, the LIP may not undergo an endogenous increase during ferroptosis, and that transcriptional regulation of iron genes may not be a primary driver of ferroptosis sensitivity.

The labile iron pool is not altered during ferroptosis

Previous studies have shown that cellular iron increases following the initiation of ferroptosis, primarily through the degradation of ferritin via ferritinophagy[18,19]. These studies measured LIP by relying on fluorescent probes such as Calcein AM[33–35] and PhenGreen SK[36]. These probes measure LIP by introducing a nonfluorescent iron chelator that displaces iron bound to the probe, leading to dequenching. The extent of which the dequenching occurs is used in reference to a fluorescence calibration standard through which the LIP concentration can be inferred. These methods present several limitations and technical challenges[35,37,38].

To assess the LIP during ferroptosis induction, we utilized a reactivity-based probe known as TRX-PURO. This probe is designed to detect free, redox-active iron without interfering with protein-bound iron[37]. TRX-PURO consists of a "caged" puromycin molecule that is selectively activated (uncaged) upon reaction with labile iron. When the cage is removed by free iron, the released puromycin becomes incorporated into nascent polypeptides at the ribosome. The incorporated puromycin can then be detected via western blot using α-puromycin antibodies (Figure 4A). As the concentration of labile iron increases, more TRX-PURO molecules are uncaged, resulting in greater puromycin incorporation. This makes TRX-PURO a robust and sensitive tool for detecting dynamic changes in the LIP. We validated this probe in HEK293 cells by treating them with increasing concentrations of FAC (10, 25, 50 µM) to elevate the LIP (Figure 4B). Puromycin incorporation increased dose-dependently with FAC, consistent with elevated labile iron levels. Co-treatment with the iron chelator deferoxamine (DFO) reduced puromycin incorporation back to baseline, confirming the specificity of the probe for free iron.

To investigate whether the LIP changes endogenously during ferroptosis we added TRX-PURO in addition to RSL3, JKE, and IKE for 16 hours (Figure 4C-E). RSL3 treatment did not significantly alter puromycin incorporation in HCT116, SW480, or RKO cells, and only a modest increase was observed in HT1080 cells at the highest RSL3 concentration (2.5 µM) (Figure 4C). JKE treatment had no effect on LIP in any of the cell lines (Figure 4D), and IKE caused only a slight increase in labile iron levels (Figure 4E). Together, these results demonstrate that while ferroptotic inducers alter iron homeostasis gene expression, they do not consistently increase the LIP, suggesting that an endogenous rise in LIP is not a conserved feature of ferroptosis.

Discussion

Ferroptosis is a form of regulated cell death that depends on iron and is characterized by the accumulation of lipid peroxides[10]. Unlike apoptosis or necroptosis, ferroptosis lacks well-defined molecular markers. Additionally, whether endogenous mediators regulate ferroptosis is poorly understood. Among these regulators is thought to be iron and particularly the LIP. The LIP plays a central role by triggering the Fenton reaction and initiating lipid peroxidation[39]. However, the

extent to which endogenous fluctuations in iron availability through the LIP directly contribute to ferroptosis remains unknown.

Our data confirms that iron remains functionally essential for ferroptosis. When we increased intracellular iron levels through exogenous supplementation with FAC, CRC cells became markedly more sensitive to ferroptosis inducers. This synergy was observed in multiple ferroptosis-sensitive and -resistant CRC cell lines and the ferroptosis-sensitive HT1080 fibrosarcoma cell line. Despite the reliance on iron for triggering ferroptosis our results suggest CRC cells may not potentiate ferroptosis through iron mobilization but instead exhibit a relatively stable LIP. The minimal transcriptional response of iron homeostasis genes (TRFC, DMT1, FTH1, FPN) suggests that ferroptosis initiation in these cells does not trigger broad changes in iron homeostasis, at least within the early time points examined. Taken together these results highlight an important distinction: while ferroptosis in CRC cells requires iron, the endogenous regulation of the LIP may not be the primary determinant of ferroptotic potentiation. This could be reflective of an adaptive mechanism to limit oxidative damage or a context-specific regulation in iron metabolism unique to CRC.

The compartmentalization of iron in subcellular compartments may also contribute to ferroptosis in ways not captured by bulk cytosolic LIP measurements. Recent work by Cañeque et al. demonstrates that activating lysosomal iron triggers ferroptosis in cancer cells, particularly affecting drug-tolerant persister populations[40]. This finding suggests that compartment-specific iron pools, such as lysosomal iron, play a pivotal role in ferroptosis regulation. Our observation that the cytosolic LIP remains stable during ferroptosis further supports the idea that iron compartmentalization, rather than total iron levels, may be critical in determining ferroptosis sensitivity.

Therapeutically, our work supports the strategy of leveraging exogenous iron supplementation to enhance the efficacy of ferroptosis-inducing agents in CRC. Many tumors including CRC, are characterized by elevated iron accumulation[14–17], which suggests mechanisms to buffer excess redox-active iron to avoid cytotoxicity. Identifying and targeting these iron-buffering pathways could represent an approach to increase the tumor sensitivity to ferroptosis-inducing therapies.

In summary, our study reveals that while exogenous iron can synergize with ferroptosis inducers in CRC, the LIP does not increase endogenously during ferroptosis. These findings redefine the assumed role of LIP dynamics in ferroptosis potentiation and open new avenues for ferroptosis-based cancer therapy. Future studies should investigate whether targeting iron compartmentalization or buffering systems can enhance ferroptosis sensitivity in CRC and other iron-dependent cancers.

Methods

Drugs

RSL3, JKE1674, and IKE were prepared fresh from powder prior to use and diluted in DMSO. RSL3, JKE1674, and IKE were stored with a stock concentration of 10 mM in DMSO at -20°C. TRX-PURO was stored with a stock concentration of 4 mM in DMSO at -20°C. All final concentrations for experiments were prepared in cell culture media.

Cell lines

Human intestinal colon cancer cell lines HCT116, SW480, RKO along with human embryonic kidney cells HEK293T, and fibrosarcoma cells HT1080 were utilized. All cell lines were cultured

in complete DMEM medium supplemented with 10% fetal bovine serum and 1% antibiotic/antimycotic solution, maintained at 37°C in an atmosphere of 5% CO_2 and 21% O_2.

Cell growth and synergy assays

Cells were plated between 250-500 cells/well and were allowed to adhere overnight, imaged for a day 0 reading and then immediately treated as indicated in the figure legend. Images were acquired 72 hours after treatment for final reading. Imaging was done on the Cytation 5 Imaging Multi-Mode reader with attached BioSpa from Agilent BioTek. Cytation software was used to quantify the cell count.

Analysis was performed by normalization to cell number at first reading (day 0) - all wells plated were averaged for analysis. Graphs were plotted using Prism with error bars representing mean +/- standard deviation.

To determine synergy between two different compounds, technical replicates of control and drug treatment wells within a plate were averaged. Fold changes relative to the averaged vehicle treatment group were calculated and then converted to a percentage to represent percent viability. The percent viability of the control groups (Vehicle, 250 uM, 500 uM, 1000 uM FAC) were then averaged to use as control values in the synergy analysis. These values were then used to determine synergy by the Bliss independence dose-response surface model using the SynergyFinder+ web application[14].

qPCR

Cell lines were treated for 16 hours and RNA was extracted using the Trizol reagent. RNA yield was then quantified using a Nanodrop. 1 µg of RNA was reverse transcribed to cDNA using the Invitrogen SuperScriptTM III First-Strand Synthesis System. After cDNA was collected Real time (RT) PCR reactions were done using three technical replicates for each sample. Then cDNA gene specific primers and SYBR green master mix were combined and then run on the Applied BioSystems QuantStudio 5 Real-Time PCR System. GAPDH was used as the housekeeping gene to calculate fold-change of the genes using the ΔΔCt method.

DMT1 F: CCTGTGGCTAATGGTGGAGTTGG
DMT1 R: GGAGATTGATGGCGATGGCTGAC
TRFC1 F: AGTTGAACAAAGTGGCACGAG
TRFC1 R: GCAGTTGGCTGTTGTACCTC
FTH1 F: TCCTACGTTTACCTGTCCATG
FTH1 R: GTTTGTGCAGTTCCAGTAGTG
FPN F: CACAACCGCCAGAGAGGATG
FPN R: CACATCCGATCTCCCCAAGT

Western Blot

Cells were seeded in a 12-well plate each condition and allowed to adhere overnight. Cells were plated to reach ~0.4x10^6 cells/well at time of harvest. After adherence cells were treated for 16 hours with RSL3, JKE1674, IKE, and with or without TRX PURO (1 µM). Cells were then lysed with RIPA assay buffer with added protease (1:100 dilution; MilliporeSigma) and phosphatase (1:100 dilution; Thermo Fisher Scientific) inhibitors. Lysates were quantified by BCA protein assay kit (Pierce – Thermo Fisher Scientific) and normalized for loading. Solubilized proteins were resolved on 10% SDS-polyacrylamide gels and transferred to nitrocellulose membrane, blocked with 5% milk in TBST, and immunoblotted with the indicated primary antibodies: Actin (1:1000) (Proteintech 66009-1-Ig), and α-puromycin (1:1000) (PMY-2A4). Horseradish peroxidase–conjugated secondary antibodies anti mouse (1:2500) were purchased from Cell

Signaling (7076, 7074) and ThermoFisher Scientific (A15999). Immunoblots were imaged using the iBright imaging system.

Statistical Analysis

Results are expressed as the mean +/- standard error of the mean for all figures unless otherwise noted. Significance between 2 groups was tested using a 2 tailed unpaired t test. Significance among multiple groups was tested using a one-way ANOVA. For all ANOVAs the Tukey-Kramer test was used for posthoc multiple comparison. GraphPad Prism 10.0 was used for the statistical analysis. Biorender was used to create all the schematics. Statistical significance is described in the figure legends as: $*p < 0.05$, $** p < 0.01$, $*** p < 0.001$, $**** p < 0.0001$.

Author Contributions

VP, PPH, YMS: conceived and designed the study; VP, DRR, SS, PPH, YMS: developed the methodologies; VP, DRR, ZHL, NKD, LZ, KB: acquired the data; VP, DRR, PPH, YMS: analyzed and interpreted the data; ARR provided TRX-PURO; VP, PPH, YMS: supervised the study and wrote the manuscript; and all authors: read and approved the final manuscript.

Acknowledgements and Funding

The authors would like to acknowledge the members of the Shah and Hsu laboratories for project feedback and technical expertise. This work was supported by NIH grants R01CA148828, R01CA245546, and R01DK095201 to YMS. The work was supported by the University of Michigan Comprehensive Cancer Center Core grant P30CA046592. VP is also supported by NCI diversity supplement as part of the parent R01CA245546.

References

1. Galy, B., Conrad, M. & Muckenthaler, M. Mechanisms controlling cellular and systemic iron homeostasis. *Nat. Rev. Mol. Cell Biol.* **25**, 133–155 (2024).
2. Jandl, J. H. & Katz, J. H. The plasma-to-cell cycle of transferrin. *J. Clin. Invest.* **42**, 314–326 (1963).
3. Ohgami, R. S. *et al.* Identification of a ferrireductase required for efficient transferrin-dependent iron uptake in erythroid cells. *Nat. Genet.* **37**, 1264–1269 (2005).
4. Paradkar, P. N., Zumbrennen, K. B., Paw, B. H., Ward, D. M. & Kaplan, J. Regulation of Mitochondrial Iron Import through Differential Turnover of Mitoferrin 1 and Mitoferrin 2. *Mol. Cell. Biol.* **29**, 1007–1016 (2009).
5. Donovan, A. *et al.* Positional cloning of zebrafish ferroportin1 identifies a conserved vertebrate iron exporter. *Nature* **403**, 776–781 (2000).

6. Harrison, P. M. & Arosio, P. The ferritins: molecular properties, iron storage function and cellular regulation. *Biochim. Biophys. Acta* **1275**, 161–203 (1996).
7. Mancias, J. D., Wang, X., Gygi, S. P., Harper, J. W. & Kimmelman, A. C. Quantitative proteomics identifies NCOA4 as the cargo receptor mediating ferritinophagy. *Nature* **509**, 105–109 (2014).
8. Das, N. K. *et al.* Modulation of the HIF2α-NCOA4 axis in enterocytes attenuates iron loading in a mouse model of hemochromatosis. *Blood* **139**, 2547–2552 (2022).
9. Yang, W. S. & Stockwell, B. R. Synthetic Lethal Screening Identifies Compounds Activating Iron-Dependent, Nonapoptotic Cell Death in Oncogenic-RAS-Harboring Cancer Cells. *Chem. Biol.* **15**, 234–245 (2008).
10. Dixon, S. J. *et al.* Ferroptosis: An Iron-Dependent Form of Nonapoptotic Cell Death. *Cell* **149**, 1060–1072 (2012).
11. Winterbourn, C. C. Toxicity of iron and hydrogen peroxide: the Fenton reaction. *Toxicol. Lett.* **82–83**, 969–974 (1995).
12. Wu, J. *et al.* Intercellular interaction dictates cancer cell ferroptosis via NF2–YAP signalling. *Nature* **572**, 402–406 (2019).
13. Jiang, X., Stockwell, B. R. & Conrad, M. Ferroptosis: mechanisms, biology and role in disease. *Nat. Rev. Mol. Cell Biol.* **22**, 266–282 (2021).
14. Schwartz, A. J. *et al.* Hepcidin sequesters iron to sustain nucleotide metabolism and mitochondrial function in colorectal cancer epithelial cells. *Nat. Metab.* **3**, 969–982 (2021).
15. Liu, Z. *et al.* Iron promotes glycolysis to drive colon tumorigenesis. *Biochim. Biophys. Acta Mol. Basis Dis.* **1869**, 166846 (2023).
16. Chen, B. *et al.* PTEN-induced kinase PINK1 supports colorectal cancer growth by regulating the labile iron pool. *J. Biol. Chem.* **299**, 104691 (2023).
17. Singhal, R. *et al.* HIF-2α activation potentiates oxidative cell death in colorectal cancers by increasing cellular iron. *J. Clin. Invest.* **131**, e143691, 143691 (2021).

18. Gao, M., Monian, P., Quadri, N., Ramasamy, R. & Jiang, X. Glutaminolysis and Transferrin Regulate Ferroptosis. *Mol. Cell* **59**, 298–308 (2015).
19. Gao, M. *et al.* Ferroptosis is an autophagic cell death process. *Cell Res.* **26**, 1021–1032 (2016).
20. Yang, W. S. *et al.* Regulation of Ferroptotic Cancer Cell Death by GPX4. *Cell* **156**, 317–331 (2014).
21. DeAngelo, S. L. *et al.* Recharacterization of RSL3 reveals that the selenoproteome is a druggable target in colorectal cancer. Preprint at https://doi.org/10.1101/2024.03.29.587381 (2024).
22. Liu, Q., Yin, X., Languino, L. R. & Altieri, D. C. Evaluation of Drug Combination Effect Using a Bliss Independence Dose–Response Surface Model. *Stat. Biopharm. Res.* **10**, 112–122 (2018).
23. Seiler, A. *et al.* Glutathione Peroxidase 4 Senses and Translates Oxidative Stress into 12/15-Lipoxygenase Dependent- and AIF-Mediated Cell Death. *Cell Metab.* **8**, 237–248 (2008).
24. Das, N. K. *et al.* Microbial Metabolite Signaling Is Required for Systemic Iron Homeostasis. *Cell Metab.* **31**, 115-130.e6 (2020).
25. Rouault, T. A. *et al.* Cloning of the cDNA encoding an RNA regulatory protein--the human iron-responsive element-binding protein. *Proc. Natl. Acad. Sci.* **87**, 7958–7962 (1990).
26. Leibold, E. A. & Munro, H. N. Cytoplasmic protein binds in vitro to a highly conserved sequence in the 5’ untranslated region of ferritin heavy- and light-subunit mRNAs. *Proc. Natl. Acad. Sci.* **85**, 2171–2175 (1988).
27. Aziz, N. & Munro, H. N. Iron regulates ferritin mRNA translation through a segment of its 5’ untranslated region. *Proc. Natl. Acad. Sci.* **84**, 8478–8482 (1987).
28. Owen, D. & Kühn, L. C. Noncoding 3′ sequences of the transferrin receptor gene are required for mRNA regulation by iron. *EMBO J.* **6**, 1287–1293 (1987).

29. Mastrogiannaki, M. *et al.* HIF-2α, but not HIF-1α, promotes iron absorption in mice. *J. Clin. Invest.* **119**, 1159–1166 (2009).
30. Shah, Y. M., Matsubara, T., Ito, S., Yim, S.-H. & Gonzalez, F. J. Intestinal Hypoxia-Inducible Transcription Factors Are Essential for Iron Absorption following Iron Deficiency. *Cell Metab.* **9**, 152–164 (2009).
31. Anandhan, A. *et al.* NRF2 controls iron homeostasis and ferroptosis through HERC2 and VAMP8. *Sci. Adv.* **9**, eade9585 (2023).
32. Zhang, D. D. Thirty years of NRF2: advances and therapeutic challenges. *Nat. Rev. Drug Discov.* **24**, 421–444 (2025).
33. Cabantchik, Z. I., Glickstein, H., Milgram, P. & Breuer, W. A Fluorescence Assay for Assessing Chelation of Intracellular Iron in a Membrane Model System and in Mammalian Cells. *Anal. Biochem.* **233**, 221–227 (1996).
34. Kakhlon, O. & Cabantchik, Z. I. The labile iron pool: characterization, measurement, and participation in cellular processes1 1This article is part of a series of reviews on “Iron and Cellular Redox Status.” The full list of papers may be found on the homepage of the journal. *Free Radic. Biol. Med.* **33**, 1037–1046 (2002).
35. Epsztejn, S., Kakhlon, O., Glickstein, H., Breuer, W. & Cabantchik, I. Fluorescence analysis of the labile iron pool of mammalian cells. *Anal. Biochem.* **248**, 31–40 (1997).
36. Petrat, F., Rauen, U. & De Groot, H. Determination of the Chelatable Iron Pool of Isolated Rat Hepatocytes by Digital Fluorescence Microscopy Using the Fluorescent Probe, Phen Green Sk. *Hepatology* **29**, 1171–1179 (1999).
37. Spangler, B. *et al.* A reactivity-based probe of the intracellular labile ferrous iron pool. *Nat. Chem. Biol.* **12**, 680–685 (2016).
38. Prus, E. & Fibach, E. Flow cytometry measurement of the labile iron pool in human hematopoietic cells. *Cytometry A* **73A**, 22–27 (2008).

39. Stockwell, B. R. Ferroptosis turns 10: Emerging mechanisms, physiological functions, and therapeutic applications. *Cell* **185**, 2401–2421 (2022).
40. Cañeque, T. *et al.* Activation of lysosomal iron triggers ferroptosis in cancer. *Nature* (2025) doi:10.1038/s41586-025-08974-4.

Figure Legends

Figure 1: *Exogenous iron sensitizes CRC cells to JKE-induced ferroptosis*

(A) Cell viability of HCT116, SW480, RKO, and HT1080 cells following treatment with 2.5 μM JKE1674 after 72 hours
(B) Cell viability of HCT116, SW480, RKO, and HT1080 cells following treatment with 2.5 μM JKE1674 with the addition of 250, 500, 100 μM FAC after 72 hours
(C) Heatmap plot of synergy in HCT116, SW480, RKO, and HT1080 cells treated with JKE1674 and FAC $*p < 0.05$, $**p < 0.01$, $***p < 0.001$, $****p < 0.0001$ unless otherwise indicated. Data are presented as mean ± SEM.

Supplemental Figure 1: *Exogenous iron sensitizes CRC cells to JKE-induced ferroptosis at lower concentrations of JKE*

(A) Cell viability of HCT116, SW480, RKO, and HT1080 cells following treatment with 1.25 and 0.625 μM JKE1674 after 72 hours
(B) Cell viability of HCT116, SW480, RKO, and HT1080 cells following treatment with 1.25 and 0.625 μM JKE1674 with the addition of 250, 500, 100 μM FAC after 72 hours $*p < 0.05$, $**p < 0.01$, $***p < 0.001$, $****p < 0.0001$ unless otherwise indicated. Data are presented as mean ± SEM.

Figure 2: *Exogenous iron potentiates RSL3 and IKE-induced ferroptosis in CRC cells*

(A) Cell viability of HCT116, SW480, RKO, and HT1080 cells following treatment with 1 μM RSL3 after 72 hours
(B) Cell viability of HCT116, SW480, RKO, and HT1080 cells following treatment with 2.5 μM IKE with the addition of 250, 500, 1000 μM FAC after 72 hours
(C) Heatmap plot of synergy in HCT116, SW480, RKO, and HT1080 cells treated with RSL3 and FAC
(D) Heatmap plot of synergy in HCT116, SW480, RKO, and HT1080 cells treated with IKE and FAC $*p < 0.05$, $**p < 0.01$, $***p < 0.001$, $****p < 0.0001$ unless otherwise indicated. Data are presented as mean ± SEM.

Supplementary Figure 2: *Exogenous iron sensitizes CRC cells to JKE-induced ferroptosis at lower concentrations of RSL3 and IKE*

(A) Cell viability of HCT116, SW480, RKO, and HT1080 cells following treatment with 1.25 and 0.625 μM RSL3 after 72 hours
(B) Cell viability of HCT116, SW480, RKO, and HT1080 cells following treatment with 1.25 and 0.625 μM IKE with the addition of 250, 500, 100 μM FAC after 72 hours $*p < 0.05$, $**p < 0.01$, $***p < 0.001$, $****p < 0.0001$ unless otherwise indicated. Data are presented as mean ± SEM.

Figure 3: *Iron homeostatic genes are not altered in RSL3, JKE, and IKE-induced ferroptosis in CRC cells*

(A) qPCR of iron homeostasis genes in HCT116, SW480, RKO, and HT1080s treated with 0.25, 0.5, and 1 μM RSL3 after 16 hours
(B) qPCR of iron homeostasis genes in HCT116, SW480, RKO, and HT1080s treated with 0.25, 0.5, and 1 μM JKE1674 after 16 hours

Figure 4: *The labile iron pool is not altered during ferroptosis*

(A) Schematic of mechanism of puromycin (PURO) release from TRX-PURO and incorporation into nascent proteins at ribosome

(B) Validation of TRX-PURO by western blot to assess labile iron pool concentration
(C) Western blot of HCT116, SW480, HT1080, RKOs to assess labile iron pool concentration after treatment of 1, 0.5, 0.25 μM RSL3
(D) Western blot of HCT116, SW480, HT1080, RKOs to assess labile iron pool concentration after treatment of 2.5, 1.25, 0.625 μM JKE
(E) Western blot of HCT116, SW480, HT1080, RKOs to assess labile iron pool concentration after treatment of 2.5, 1.25, 0.625 μM IKE

FIGURE 1

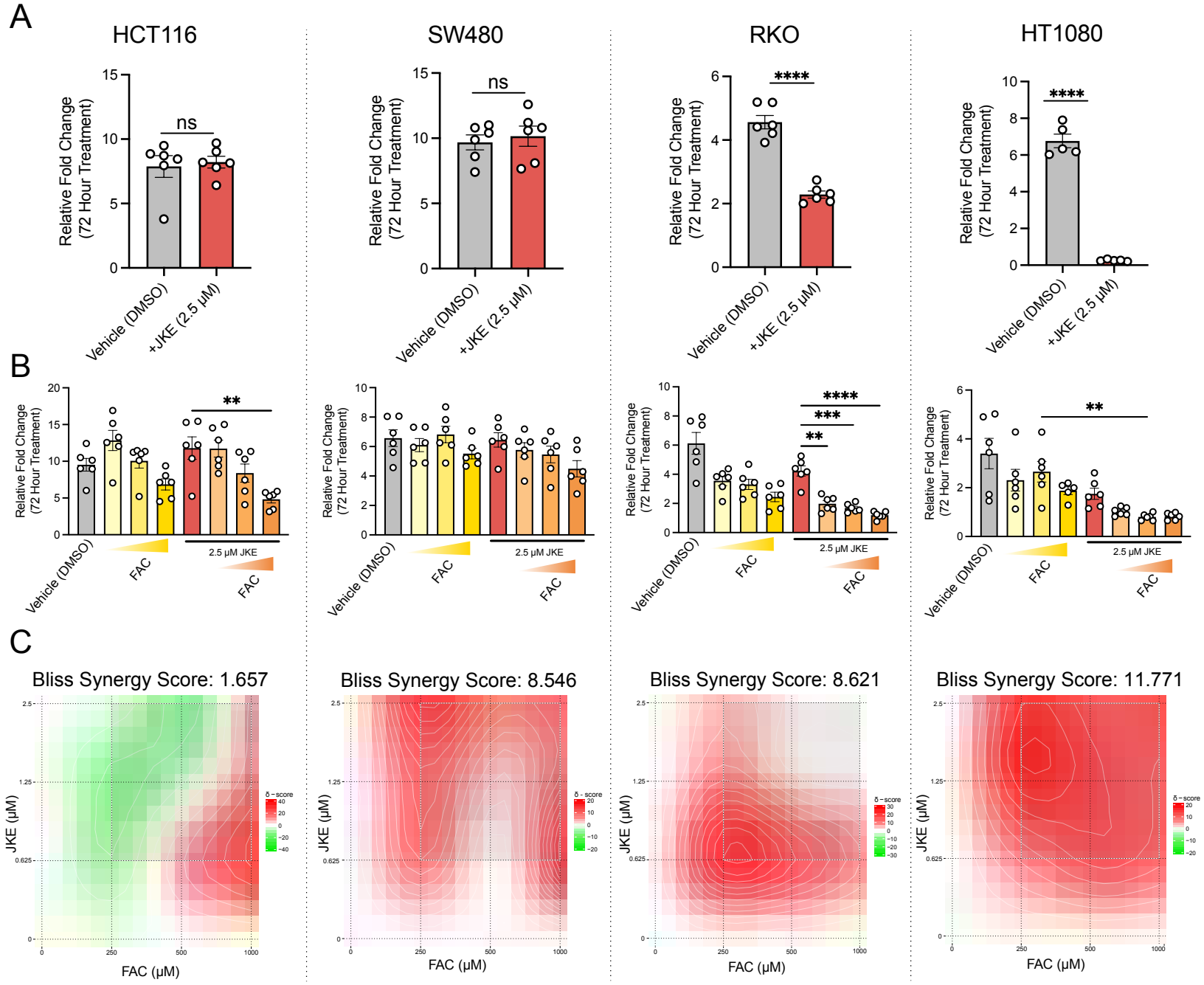
A
HCT116
SW480
RKO
HT1080
Relative Fold Change (72 Hour Treatment)
ns
****
Vehicle (DMSO)
+JKE (2.5 μM)
B
**
***
2.5 μM JKE
FAC
C
Bliss Synergy Score: 1.657
Bliss Synergy Score: 8.546
Bliss Synergy Score: 8.621
Bliss Synergy Score: 11.771
JKE (μM)
FAC (μM)
δ - score

SUPPLEMENTARY FIGURE 1

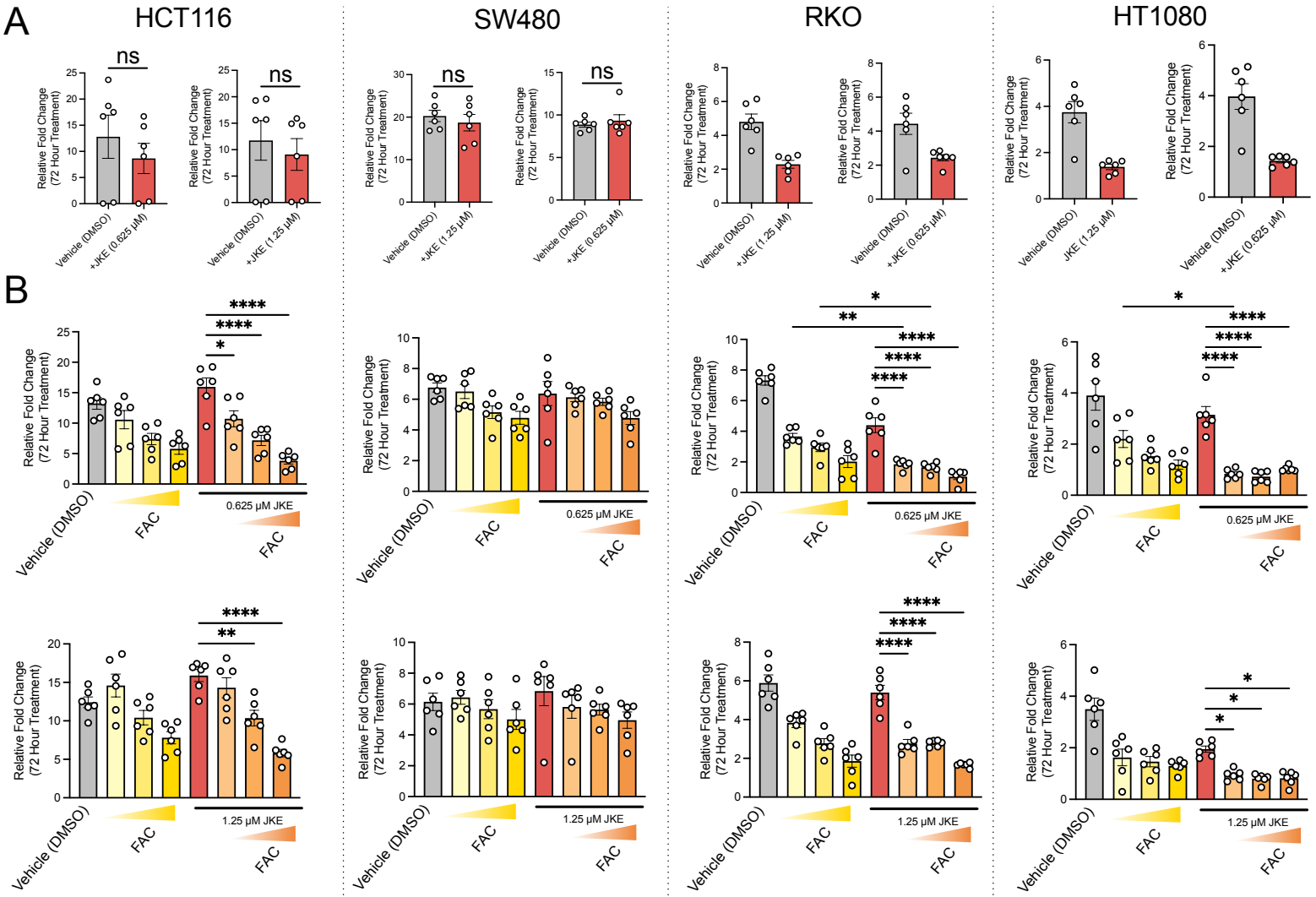

FIGURE 2

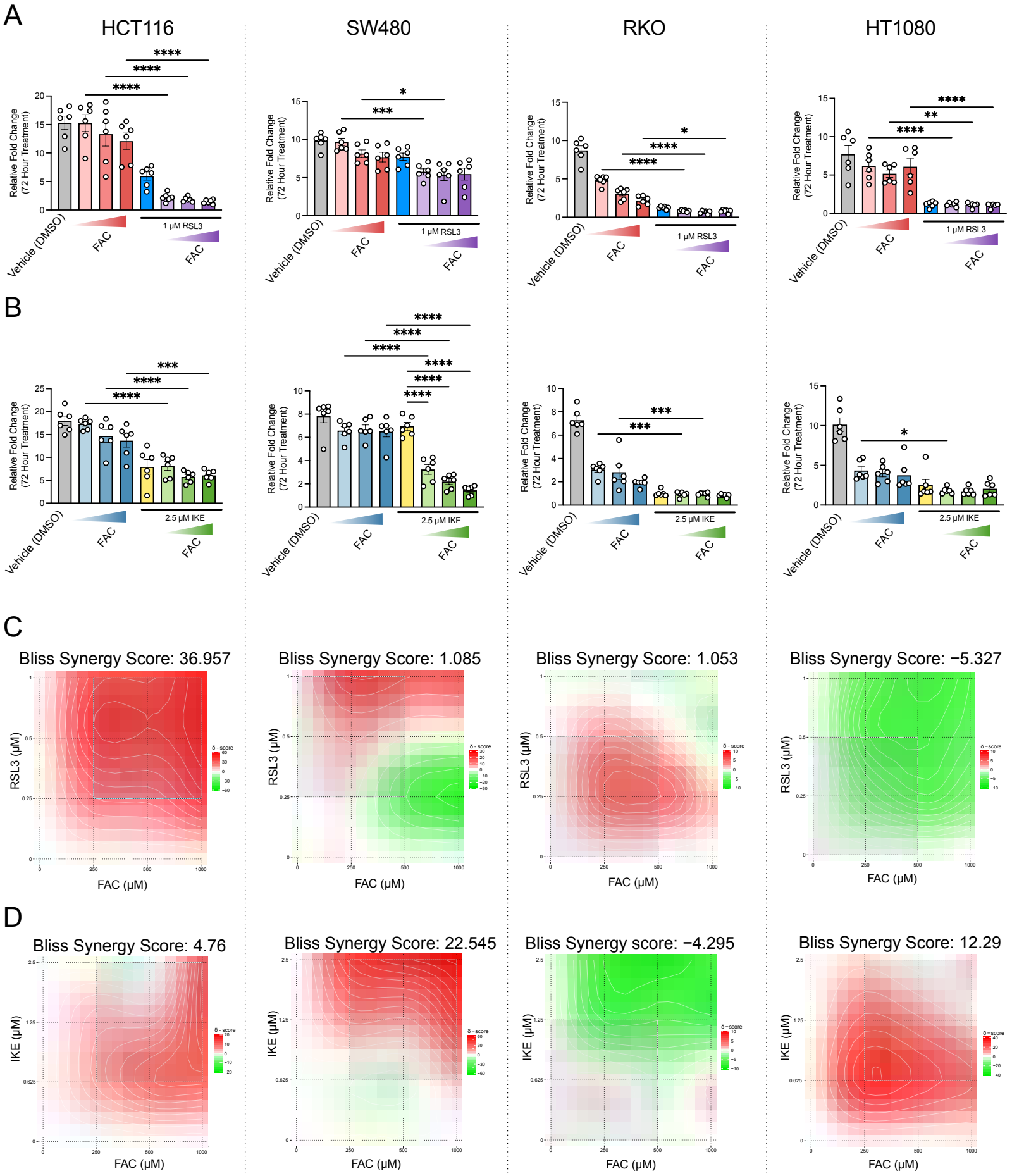
A
HCT116
SW480
RKO
HT1080
Relative Fold Change (72 Hour Treatment)
Vehicle (DMSO)
FAC
1 μM RSL3
B
2.5 μM IKE
C
Bliss Synergy Score: 36.957
Bliss Synergy Score: 1.085
Bliss Synergy Score: 1.053
Bliss Synergy Score: −5.327
RSL3 (μM)
FAC (μM)
δ - score
D
Bliss Synergy Score: 4.76
Bliss Synergy Score: 22.545
Bliss Synergy score: −4.295
Bliss Synergy Score: 12.29
IKE (μM)

SUPPLEMENTARY FIGURE 2

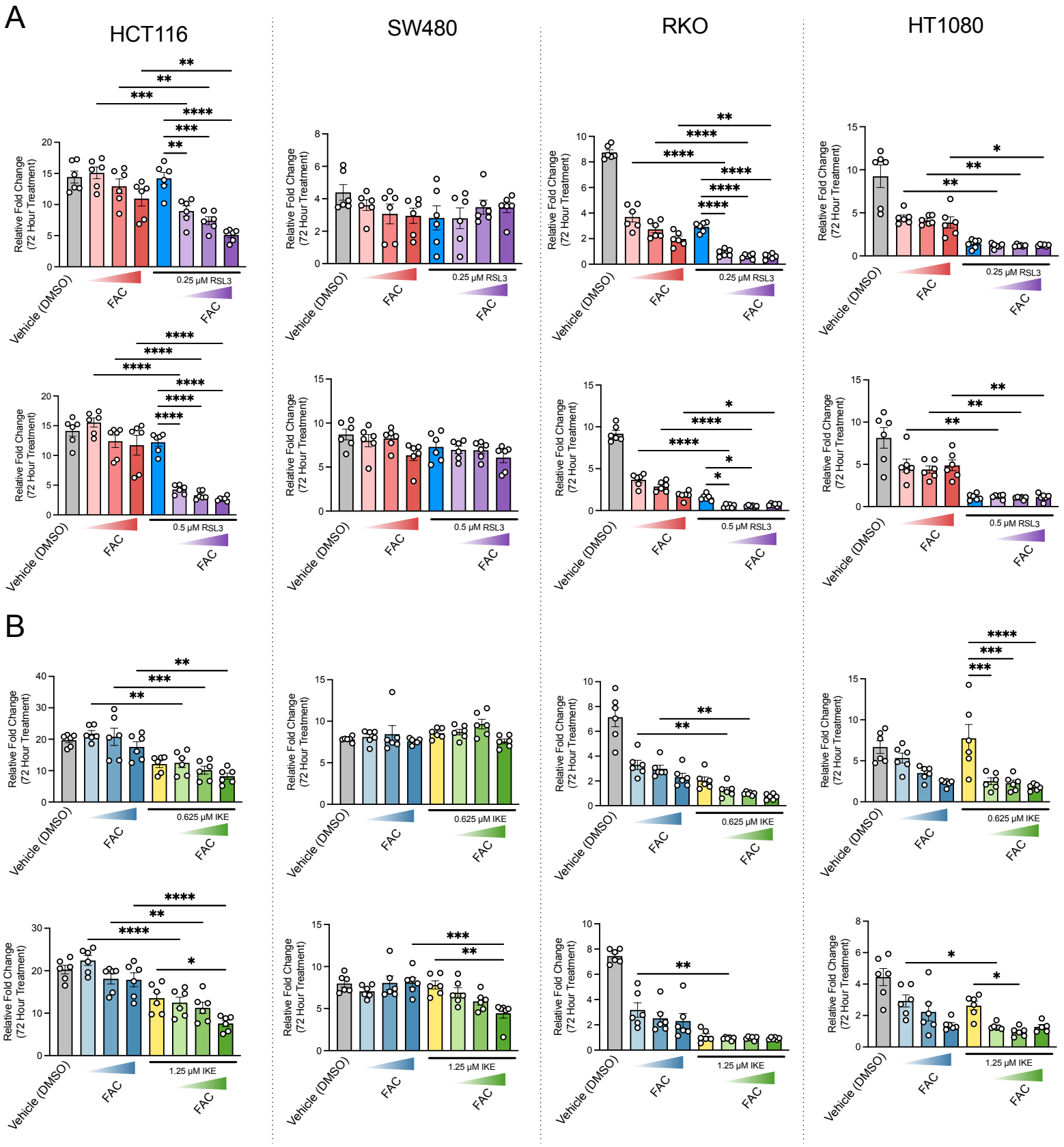

FIGURE 3

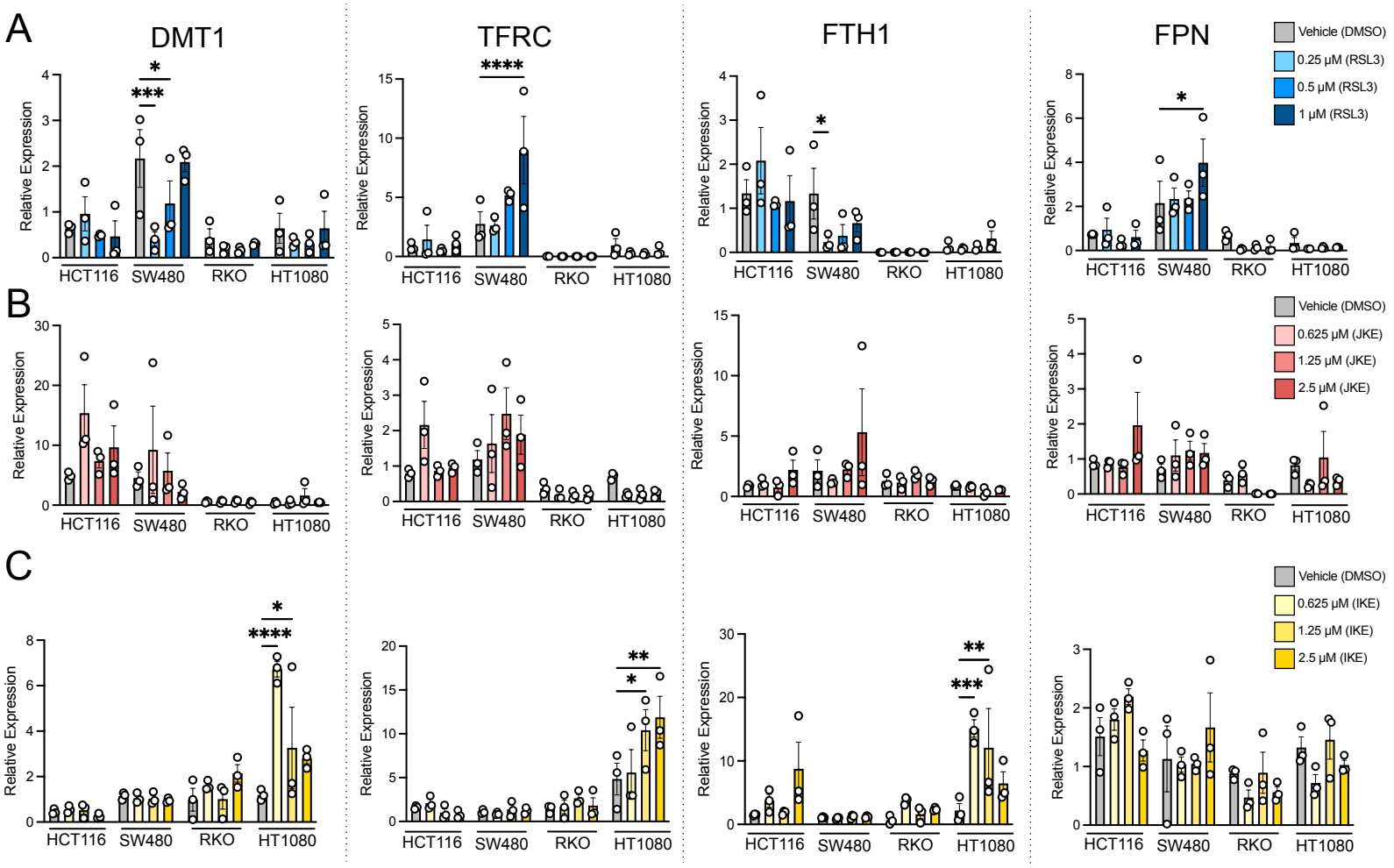
A
DMT1
TFRC
FTH1
FPN
Vehicle (DMSO)
0.25 μM (RSL3)
0.5 μM (RSL3)
1 μM (RSL3)
B
Vehicle (DMSO)
0.625 μM (JKE)
1.25 μM (JKE)
2.5 μM (JKE)
C
Vehicle (DMSO)
0.625 μM (IKE)
1.25 μM (IKE)
2.5 μM (IKE)
Relative Expression
HCT116
SW480
RKO
HT1080

FIGURE 4

A

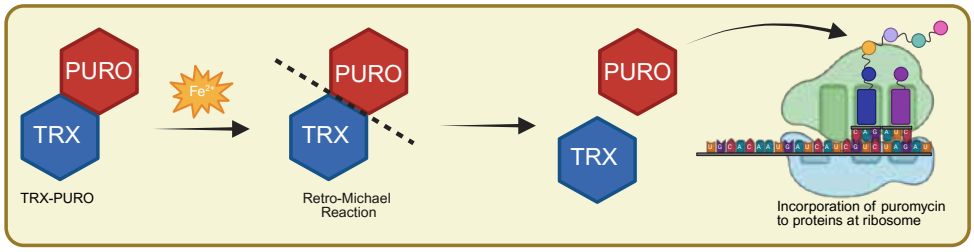

B

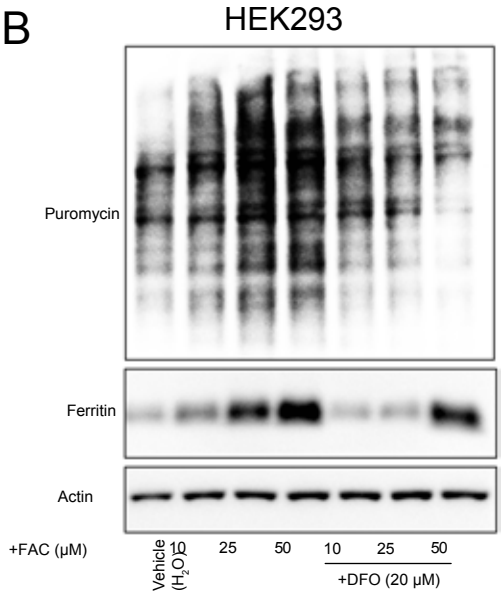

C

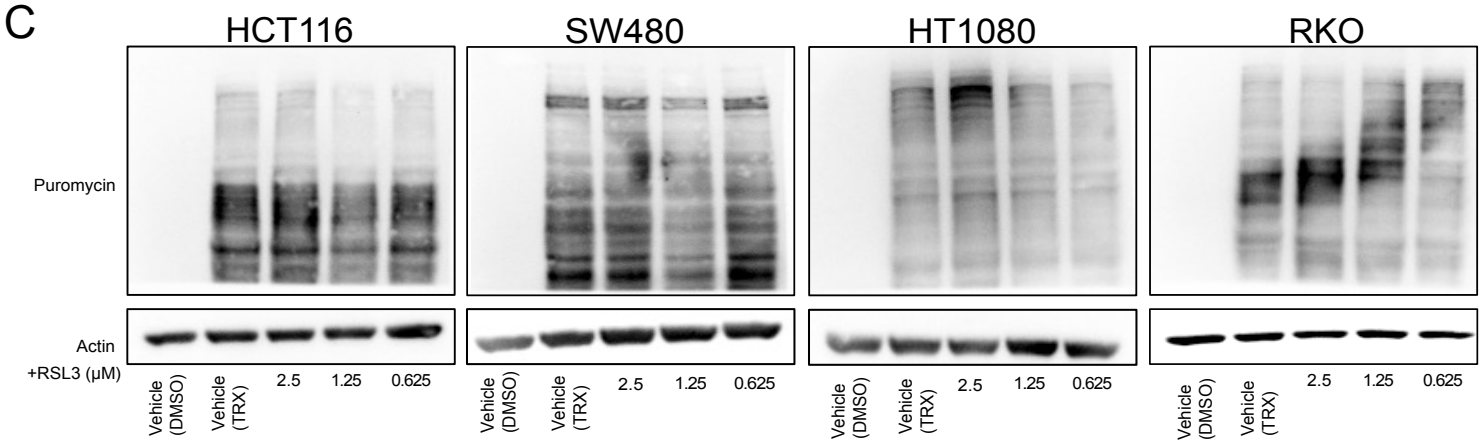

D

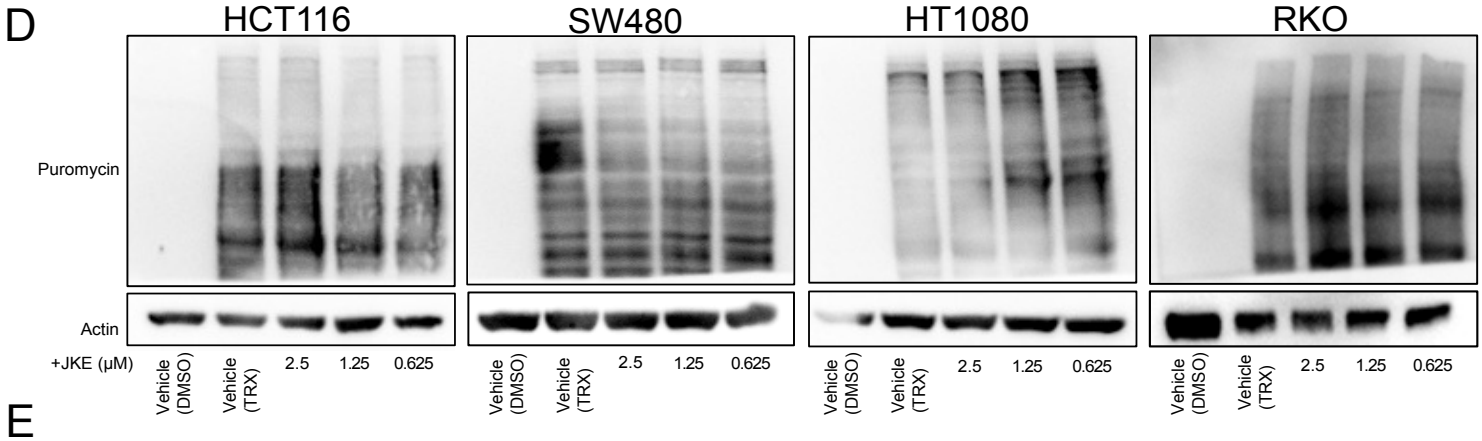
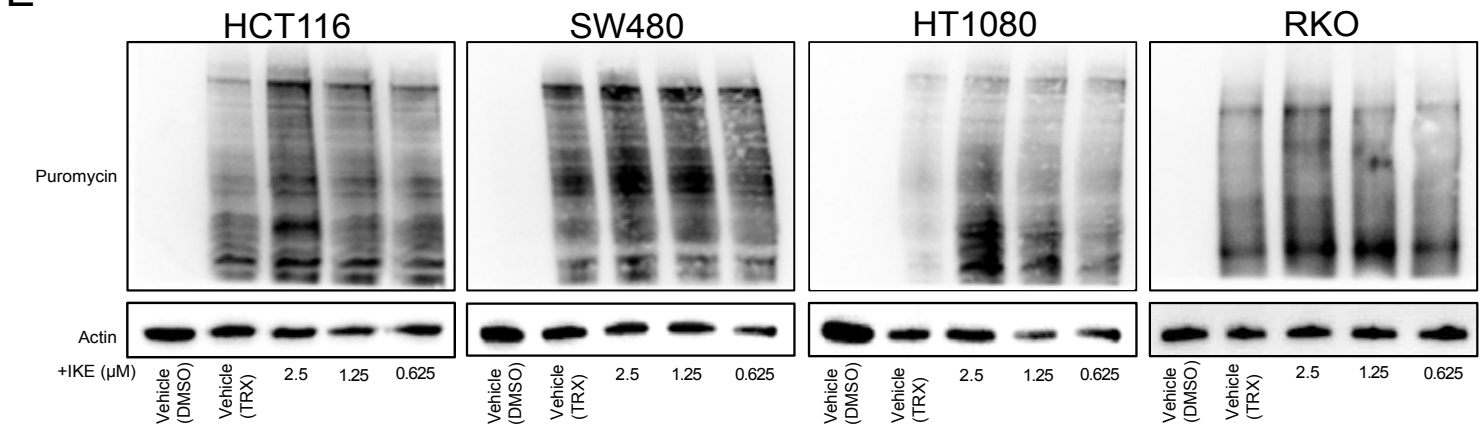
E